Exceeding 200-ns Lifetimes in Polycrystalline CdTe Solar Cells

Tursun Ablekim, Joel N Duenow, Craig L Perkins, John Moseley, Xin Zheng, Thomas Bidaud, Berengere Frouin, Stephane Collin, Matthew O Reese, Mahisha Amarasinghe, et al.

Exceeding 200-ns Lifetimes in Polycrystalline CdTe Solar Cells

Authors: T. Ablekim,[1,4] J.N. Duenow,[1] C.L. Perkins,[1] J. Moseley,[1] X. Zheng,[1,2] T. Bidaud,[3] B. Frouin,[3] S. Collin,[3] M.O. Reese,[1] M. Amarasinghe,[1,2] E. Colegrove,[1] S. Johnston,[1] W.K. Metzger[1]

Affiliations:
[1] National Renewable Energy Laboratory, Golden, Colorado 80401, USA
[2] University of Illinois at Chicago, Chicago, IL 60607, USA
[3] Centre for Nanoscience and Nanotechnology, CNRS, University Paris-Saclay, 91120 Palaiseau, France
[4] First Solar Inc., Santa Clara, CA 95050, USA

Abstract

CdTe photovoltaics has achieved one of the lowest levelized costs of electricity among all energy sources. However, for decades, carrier lifetimes have been inferior to those of other prevalent solar cell materials. This quality has inhibited common methods to improve solar cell efficiency such as back-surface fields, electron reflectors, or bifacial solar cells. In this work, we demonstrate a significant increase in carrier lifetime to values exceeding 200 ns in fully functional CdTe solar cells. The increased lifetime is achieved in these complex polycrystalline cells by realizing multiple characteristics simultaneously—the formation of oxidized tellurium species at the transparent conducting oxide interface, large CdSeTe grains at the absorber/emitter interface, and intragrain passivation in the absorber layer. The carrier lifetime is correlated to the open-circuit voltage and enables paths for back-surface manipulation and novel cell architectures to further improve CdTe photovoltaic performance.

Introduction

The quality and performance of photovoltaic materials such as Si, GaAs, perovskites, $Cu(In,Ga)Se_2$, and CdTe depend on the average time that carriers excited by sunlight are able to drift and diffuse prior to recombination.[1] Typical CdTe carrier lifetimes—several ns to tens of ns—are relatively short compared to the hundreds of ns achieved in CIGS and perovskites,[2-7] and microseconds and milliseconds achieved in GaAs and Si, respectively.[8-10] This is one reason why CdTe record solar cell efficiency is less than in these other material systems.[11] Furthermore, the resulting diffusion length limits the ability to implement back-surface passivation and carrier reflection, which are critical to existing high-efficiency Si and III-V solar cell technologies.[1] It also restricts semiconductor device designs such as bifacial and interdigitated back-contact solar cells. Increased lifetime in and of itself can improve performance. Recent modeling indicates that for typical CdTe solar cell thickness and properties, carrier lifetime exceeding about 100 ns can also enable back-surface passivation and designs to significantly increase efficiency to values as high as 28%, provided other properties are also optimized.[12] GaAs solar cells, which have a similar bandgap, have demonstrated >28% efficiency in part due to long carrier lifetime and back-surface fields;[13] but applications are limited by the low throughput, and costs/W are currently about 500–1000 times greater than those of commercial modules for residential and utility applications.[14] The high throughput of module production has positioned CdTe as a cost leader in utility photovoltaics; substantive lifetime gains can enable higher efficiency at levelized costs of electricity well below those of conventional fuels.[15]

Figure 1 illustrates a schematic of the superstrate CdTe solar cell configuration. From about 1992 to 2012, the most common *n*-type layers were either SnO_2/*i*-SnO_2 or $CdSnO_x$/$ZnSnO_x$ bilayers followed by CdS.[16,17] Carrier lifetime measured by time-resolved photoluminescence through the glass increased substantively to about 5–30 ns in typical devices when CdS was replaced with CdSeTe bandgrading; this was a key component of the increase in efficiency from 16.7% to 22.1%.[3,4,5,18-22] Eliminating CdS substantively reduced absorption of sunlight with wavelengths less than 520 nm, thereby increasing photocurrent in the blue end of the solar spectrum. At the same time, the CdSeTe alloy formed by Se diffusion during the post-deposition $CdCl_2$ anneal decreased the bandgap to ~1.4 eV, thereby increasing photocurrent in the red region of the solar spectrum. Critically, open-circuit voltage (V_{oc}) did not decrease commensurately, in large part because CdSeTe demonstrated greater lifetime than CdTe.[23]

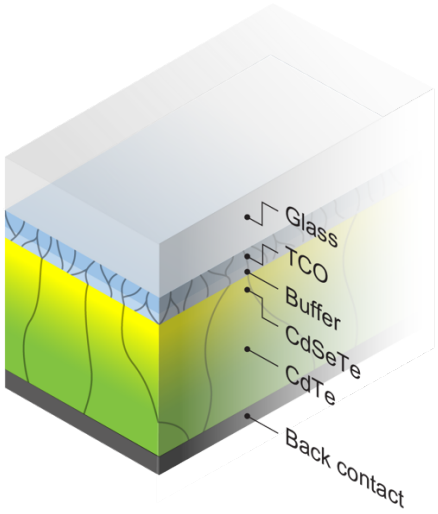

Figure 1. Schematic of a CdTe solar cell. Transparent conducting oxide (TCO) is deposited on glass, followed by different potential buffer layers as described in the text, CdSeTe, CdTe, and back-contact formation. The layers and grain size are not drawn to scale.

A fundamental challenge is that the fast deposition (few to >10 μm/min) of CdTe-based absorber material on a nanocrystalline heterointerface results in as-deposited lifetimes on the order of tens of picoseconds,[3] a poor starting point remedied only partially by recrystallization and passivation during post-deposition $CdCl_2$ or $MgCl_2$ processing.[3,24-26] Nonetheless, recent developments indicate that long lifetimes in CdTe-based material are possible. Single crystals doped with P demonstrated that bulk CdTe is capable of radiatively limited lifetimes reaching hundreds of nanoseconds, commensurate with GaAs over the ideal hole density range for solar cells.[27] In parallel, depositing thick large-grain films with standard polycrystalline equipment, growth rates, and source material revealed that CdTe lifetimes of tens of ns were possible without the $CdCl_2$ treatment, indicating that relatively low-impurity source material does not necessarily introduce lifetime-limiting impurities.[28] More recently, decay times of hundreds of nanoseconds have been observed by growing polycrystalline glass/Al_2O_3/CdSeTe/Al_2O_3 or glass/MgZnO/CdSeTe/MgZnO double heterostructures and subjecting them to a $CdCl_2$ anneal.[29] The results are promising, although multiple diffusion length measurements have yet to corroborate lifetimes in these idealized test structures, and the structures are distinct from high-efficiency polycrystalline CdTe solar cells.

Here, we examine glass/SnO_2:F/*i*-SnO_2/MgZnO/CdSeTe/CdTe cells as a function of Se composition in the CdSeTe layer. The chemistry at the MgZnO/CdSeTe interface is examined by producing atomically smooth planar cleaves in a controlled glovebox environment followed by X-ray photoelectron spectroscopy (XPS) and other measurements. The measured recombination lifetime is strongly correlated to device performance and reaches values exceeding 200 ns. The carrier lifetime is not driven by one mechanism, but instead, by a confluence of interfacial chemistry, recrystallization of large CdSeTe grains at the MgZnO/CdSeTe interface, and intragrain and grain-boundary passivation in the absorber layer.

Compositional dependence and recombination

MgZnO was deposited by sputtering on TEC12D commercial glass with SnO_2:F and nominally undoped SnO_2.[30] About 1 μm of CdSeTe was deposited by thermal evaporation from a ternary $CdSe_xTe_{1-x}$ source. The Se content was varied from 0% to 40% in increments of 10%. Afterwards, CdTe was thermally evaporated from a separate source, and the samples were subjected to a $CdCl_2$ anneal of 420ºC. Devices were completed by immersing the samples in a $CuCl_2$ solution followed by Au metallization. Figure 2 illustrates the external quantum efficiency (EQE) measured as a function of alloy composition and a representative current density-voltage (J-V) curve for Se composition of 30% with a V_{oc} of 843 mV, short-circuit current density (J_{sc}) of 29.4 mA/cm^2, and efficiency of 17%–18%.

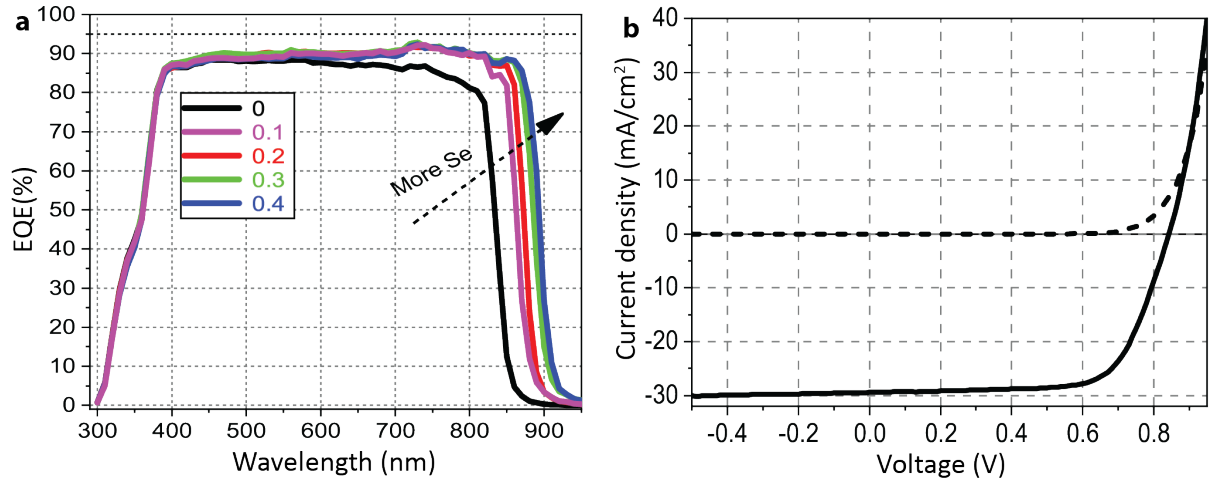

Figure 2. EQE and JV characteristics. a, EQE for solar cells with Se composition ranging from 0% to 40% indicates successively more photocurrent in the red region as the Se alloying decreases the bandgap near the MgZnO/CdSeTe interface. **b,** Typical J-V curves for Se composition corresponding to 30%.

The lifetimes were measured by time-correlated single-photon counting using a laser pulse at 640 nm incident through the glass and absorbed primarily in the CdSeTe absorber region.[31] Figure 3**a** illustrates a representative curve. The latter section of the decay curve is fit as has become customary in the field, and corresponds to a decay time exceeding 250 ns. Long decay times can be associated with traps or carrier kinetics. For example, if the electron-hole excitation is low relative to the equilibrium hole density, the *p*-*n* junction electric field separates holes and electrons to the edge of the *p*- and *n*-type regions, respectively. These carriers can then gradually leak back, recombine, and luminesce, thereby creating relatively long decay tails that are not correlated to device performance.[32] Here, the injection levels (10^{16}–10^{17} cm^{-3}) are high relative to the equilibrium carrier density, which serves to screen the electric field.[32,33] Long decay curves can also be generated by trap capture and reemission, in which case the measured lifetime is not directly related to the diffusion length and photovoltage.[34] Figure 3**b** illustrates that the V_{oc} is correlated to the logarithm of the measured carrier lifetime. This relation is consistent with basic device physics,[3,35] and it indicates that the lifetimes are not produced by an artifact unrelated to solar cell performance. Figure 3**b** also illustrates that the lifetime generally increases with increasing Se concentration until reaching a value of 30%. On average, the measured lifetime decreases as the Se level increases from 30% to 40%. By conducting different characterization experiments, it is possible to gain insight into the underlying mechanisms adjusting recombination.

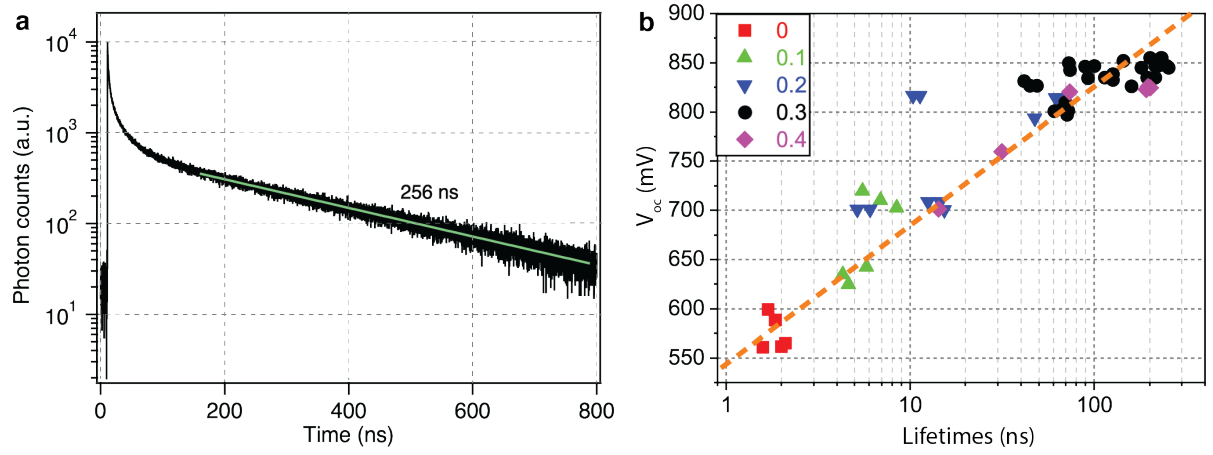

Figure 3. The correlation of lifetime and open-circuit voltage. a, Characteristic single-photon counting curve measured on a solar cell with 30% Se composition. The green line illustrates a single exponential decay fit. **b,** The correlation of lifetime *vs* V_{oc} for CdSeTe/CdTe solar cells with Se composition ranging from 0% to 40%. The straight dashed orange line serves as a guide to the eye in the linear-log plot.

Physical Mechanisms

To assess the physical mechanisms creating these very long lifetimes, we used a thermomechanical cleaving method to cleanly separate a number of devices at the MgZnO/CdSeTe interface.[36] This method exposes the critical *p-n* junction interface that changes during subsequent deposition, $CdCl_2$ annealing, and back-contact processing for examination by XPS and other surface-sensitive probes. Cleaving occurs in an argon-filled glovebox that is connected to a surface analysis cluster tool. Thus, the samples are not exposed to air, oxidation, polishing, focused-ion-beam milling, or other damaging sample preparation, enabling a unique examination of these poorly understood interfaces.

Figure 4**a** illustrates XPS spectra of the Te $3d_{5/2}$ region taken from the CdSeTe side of cleaved devices. The XPS is sensitive to depths of just several nanometers and reveals two peaks associated with Te^{2-} and Te^{4+}. The spectra in Fig. 4**a** are normalized in height to the Te^{2-} peak. The Te^{2-} stems from tellurium in the CdSeTe alloy. The Te^{4+} is oxidized tellurium that had been directly in contact with the transparent conducting oxide.[37] Such oxidized tellurium is typically found at the air-exposed surfaces of CdTe and has been associated with native oxides such as $CdTeO_3$, the thermodynamically most stable CdTe oxide.[38] Figure 4**a** demonstrates that the extent of tellurium oxidation depends on the Se content of the CdSeTe source material. In fact, adding Se, but not too much, can actually promote Te oxidation. Figure 4**b** illustrates that the ratio of $[Te^{4+}]/[Te^{2-} + Te^{4+}]$ summed from both sides of the interface is strongly correlated to carrier lifetime. Figure 4**c** illustrates that V_{oc} progressively climbs with the lifetime and $[Te^{4+}]/[Te^{2-} + Te^{4+}]$ ratio, and the V_{oc} then saturates, as predicted for absorbers with low hole density ($\sim 10^{14}$ cm^{-3}). Interestingly, the $[Te^{4+}]/[Te^{2-} + Te^{4+}]$ ratio is a better predictor of lifetime than the absorber Se composition.

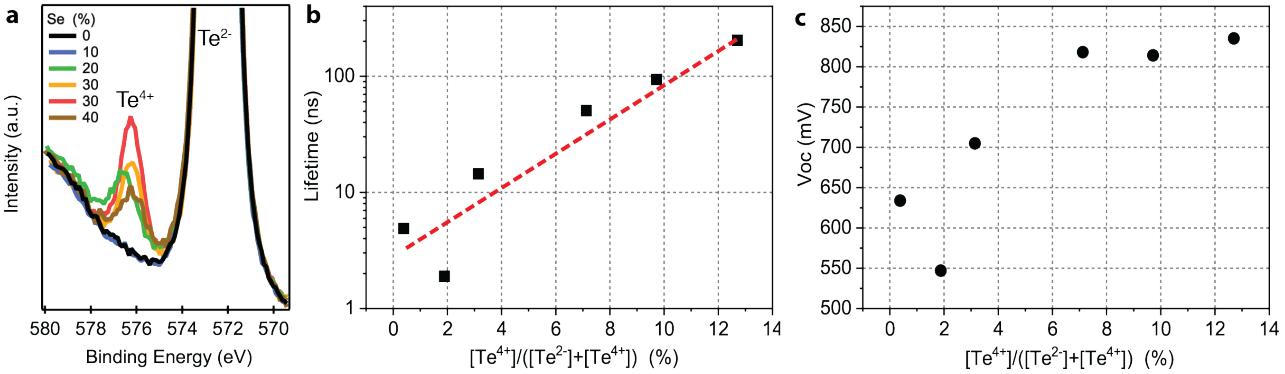

Figure 4. The relationship of Te^{4+} at the front interface with carrier lifetime and V_{oc}. a, XPS spectra at the front interface **b**, lifetime, and **c,** V_{oc} *vs* $[Te^{4+}]/[Te^{2-} + Te^{4+}]$ ratio. The red dashed line is a guide to the eye.

To image electro-optical properties across the CdSeTe and CdTe absorber, an electron beam was scanned across a beveled surface to generate electron-hole pairs with ~100-nm spatial resolution (Fig. 5**a**). Cathodoluminescence (CL) spectra were collected at each position, and the peak photon energy and intensity were averaged parallel to the junction as a function of depth into the film. Figure 5**b** illustrates that the peak photon energy successively drops with increasing Se source concentration at the CdSeTe/MgZnO interface (distance = 0 μm); for all source concentrations, the peak energy gradually climbs to values consistent with CdTe toward the back of the film. The injection levels correspond to electron-hole generation on the order of 10^{16}–10^{17} cm^{-3}, which screens the field created by an equilibrium hole density of 1×10^{14}–5×10^{14} cm^{-3} and leads to an intensity that is driven by the electron and hole carrier lifetimes.[39] Once the beam is fully within the absorber, where there is more Se, there is generally more CL intensity (Fig. 5**c**). Supplemental Fig. 1 illustrates areal CL intensity and bandgap images that corroborate these findings.

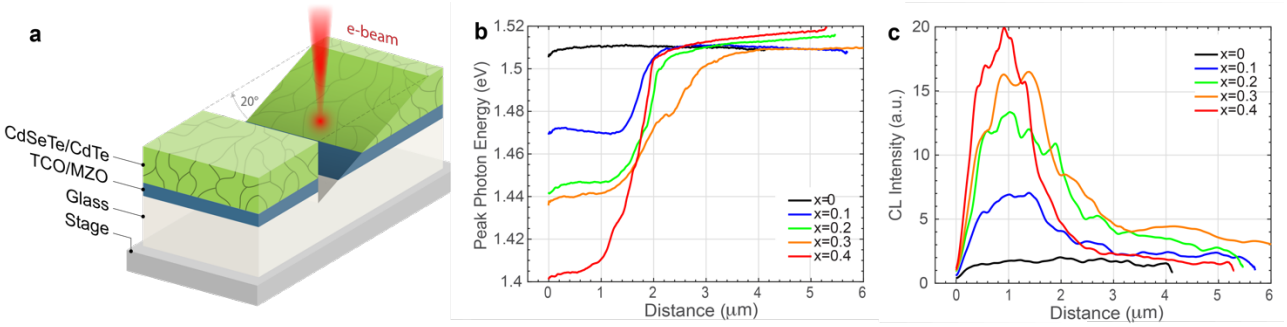

Figure 5. The correlation of peak photon energy and CL intensity with film depth. a, Schematic of CL experiment on a beveled sample. **b,** The peak photon energy and **c,** CL intensity, averaged parallel to the junction, as a function of distance from the CdSeTe/MgZnO interface.

The correlation of the CL intensity with the absorber grain structure provides more insight into the mechanisms controlling carrier lifetime. The first row of Fig. 6 illustrates CL intensity as a function of depth and Se composition using a common scale. The Attolight CL-scanning electron microscope described in the Methods section is specially designed to allow quantitative CL intensity comparisons between different samples. The CdTe (x = 0) samples appear dark due to less intensity throughout the film. For increased Se concentration at the front interface, the CL intensity similarly increases, whereas the CL intensity in the CdTe region near the back of the film remains dim. This is consistent with Se content being correlated to CL intensity and reducing recombination. The CL data in the Supplementary section reproduce these features in different sample locations on a standard parabolic mirror system, and they demonstrate that the bright bands correspond to regions where Se content shifts the bandgap. The second row in Fig. 6 shows the CL intensity scaled individually to enhance the contrast for each image. The Se bandgrading at the front interface overlaps with enhanced luminescence, and the grain-boundary intensity relative to the grain interiors is consistently dark. Because grain-boundary potentials are easily screened by the injected carriers,[40] the data indicate that the grain boundaries are defective and not fully passivated, regardless of the Se composition.

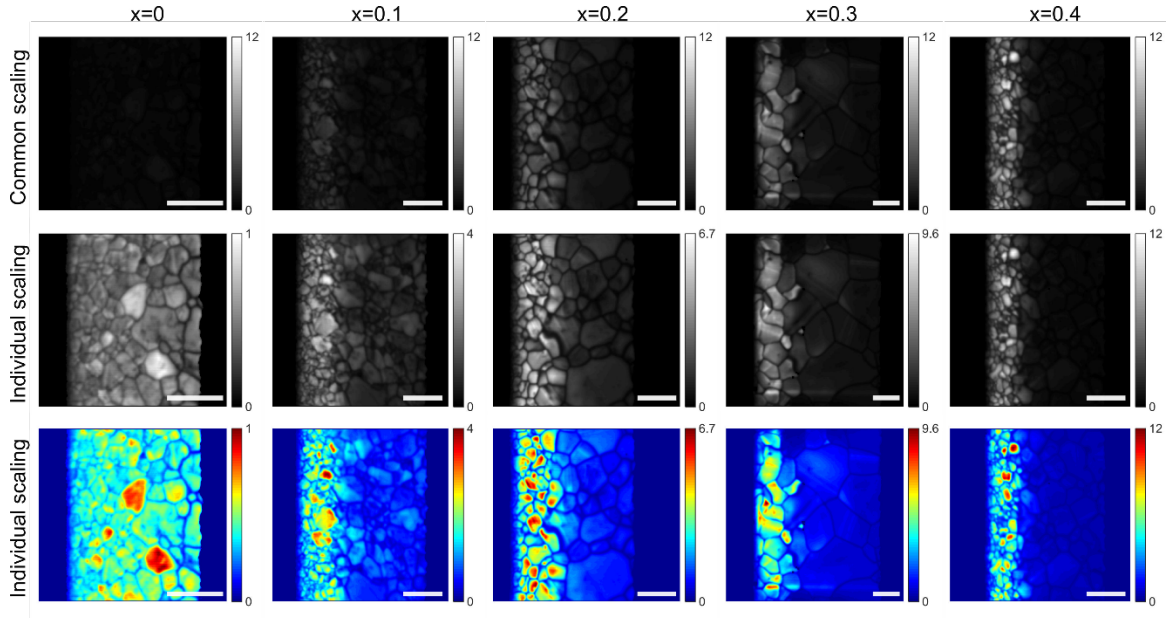

Figure 6. CL intensity contrast versus Se composition. CL intensity of beveled $CdSe_xTe_{1-x}$ samples with compositional x values ranging from 0% to 40%. The top row indicates the intensity for common scaling shown in the legend on the right. The middle row uses individual scaling for each composition to enhance the contrast for each composition. The bottom row indicates the results from the second row in color to enhance visualization throughout the film, particularly for higher Se concentration. The right-hand legend provides the scale. The white bar corresponds to 5 microns along the beveled surface.

The data illustrate another physical mechanism that can contribute to very long lifetimes. The grain structure varies as a function of Se content. Initially, as the Se composition increases, the grain size at the front interface becomes progressively larger, peaking at source compositions of 30% and then decreasing for 40%. The initial climb in grain size is correlated with carrier lifetime; however, the 40% composition shows longer lifetimes than compositions from 0% to 20%, yet fails to show significantly larger grains. The results illustrate that there are several physical mechanisms, rather than just one, that contribute to long carrier lifetime. The Se composition progressively increases intragrain CL intensity. At the same time, interfacial oxidized tellurium and grain size peak along with measured lifetime for Se contents of 30%. The optimal confluence of these multiple effects contributes to measured lifetimes in excess of 200 ns.

Conclusions

For decades, the measured carrier lifetime in high-quality CdTe solar cells has been inferior to those of current CIGS, perovskite, and GaAs solar cells. This has been one limitation to CdTe reaching the record cell efficiencies of these other technologies. This also has impeded the success of implementing back-surface fields, electron reflectors, and back-surface passivation to further increase efficiency, as well as the ability to establish new cell configurations such as bifacial or interdigitated back-contact cells. Here, lifetime values reaching 250 ns are achieved in fully functional CdTe solar cells. The long lifetimes are not easily attributed to any one physical mechanism, but instead, to several simultaneous features: the formation of a thin layer of oxidized species at the *p*-*n* junction interface, recrystallization of large CdSeTe grains at the absorber/emitter interface, and grain-boundary and intragrain recombination mitigation in the absorber layer. The carrier lifetime is correlated to the open-circuit voltage and enables paths for back-surface manipulation and novel cell architectures to further improve CdTe photovoltaic performance and reduce the costs of solar electricity.

Methods

Materials synthesis. The cell layers were deposited on NSG TEC12D soda-lime glass commercially coated with fluorine-doped tin oxide (SnO_2:F) and intrinsic tin oxide (*i*-SnO_2). MgZnO was deposited on the *i*-SnO_2 by RF sputtering from a compressed target of ZnO and MgO. The weight percent (wt%) of MgO was 4%; the remainder was ZnO. The *x* value in $Mg_xZn_{1-x}O$ films deposited from this target was about 0.08. The CdSeTe and CdTe layers were then thermally evaporated sequentially without breaking vacuum. The $CdSe_xTe_{1-x}$ source material had Se compositions ranging from x=0 to 0.4. The chamber base pressure was mid-10^{-6} Torr. The source and substrate temperatures for CdSeTe and CdTe were about 680°C and 400°C, respectively. The CdSeTe layers were nominally 1 μm thick, and the CdTe layers were 3–4 μm. After CdSeTe and CdTe deposition, the samples were $CdCl_2$-treated at 420°C for 10 minutes. Residual $CdCl_2$ was rinsed off with deionized water. The samples were then dipped in a 0.1 mMol $CuCl_2$ solution in water and annealed in a tube furnace at 200°C for 30 minutes in air. Finally, a 100-nm-thick Au contact was deposited by evaporation. The cells were isolated with mechanical scribing with a cell area of about 0.25 cm^2.

JV measurements were measured in the dark and under simulated 1-sun illumination using a Class AAA solar simulator with a Xe-arc lamp and AM1.5G filter from PV Measurements. The total cell area was measured with a system installed by the NREL Cell and Module Characterization group that uses image capture, a calibrated CNC x-y stage, and area-measurement software. The illumination intensity was calibrated using an encapsulated Si cell certified by the NREL Cell and Module Characterization group. Spectral mismatch errors based on reference and test cells are estimated to be less than 4%. The solar cells were measured in the laboratory ambient (air) and were scanned starting in the forward direction. We did not use preconditioning or observe hysteresis. Integrated absolute quantum efficiency response was measured with a Newport Oriel IQE 200 system.

Characterization. One-photon excitation time-correlated single-photon counting was performed by firing laser pulses with a wavelength of 640 nm at a rate of 1.1 MHz with a CW power of 200 μW through the glass onto the absorber layer. [31] The beam diameter was 60 μm, corresponding to an initial injection level near the absorber interface of 10^{16}–10^{17} cm^{-3}. A silicon avalanche photodiode detector was used for single-

photon detection of photons passed through interference filters to separate photoluminescence from scattered laser light. After deconvolution with the instrument system response, 20-ps lifetimes can be resolved.

Bevels for the CL measurements were prepared by focused-ion-beam milling in a xT-Nova NanoLab focused ion beam/scanning electron microscope (FIB/SEM) made by FEI Company. An ~1-µm-thick layer of protective Pt was deposited above the eventual beveled surface, which also helps to reduce "curtaining."[41] Samples were tilted 20° to the ion beam, a 30-kV beam was used to shape the bevels, and a 5-kV beam was used to clean the surfaces for CL. Surfaces were cleaned further by milling at a glancing angle with Ar^+ ions using a JEOL cross-section polisher tool operating at 3 kV. CL spectrum imaging measurements[42] were performed at room temperature in an Attolight Chronos CL-SEM.[43] Electron-beam conditions were 6-kV voltage/8-nA current. Luminescence was collected by an achromatic reflective objective (numerical aperture 0.72) that provides constant collection efficiency over a field of view of about 150 µm in diameter. Luminescence spectra were dispersed with a Horiba diffraction grating (150 grooves/mm) and recorded with an Andor Newton charge-coupled device (CCD) camera (1024×256 pixels, pixel width 26 µm). The corresponding spectral dispersion is 0.53 nm per pixel. Luminescence spectra were corrected for the diffraction efficiency of the grating and the sensitivity of the CCD camera. For Supplemental Fig. 1, CL measurements were collected on different beveled areas of the same samples in Figs. 5 and 6 at room temperature in a JEOL JSM 7600F field- emission SEM equipped with a Horiba H-CLUE CL system. The H-CLUE includes a parabolic mirror light collector, an iHR320 imaging spectrometer, and a thermoelectrically cooled Syncerity CCD camera. A grating with 300 grooves/mm and blaze at 600 nm was used. Electron-beam conditions were 7.5-kV voltage/~14-nA current.

XPS and Auger electron spectroscopy experiments were conducted in a home-built cluster tool described in Ref. 43. Using an ultra-high-vacuum (UHV)-compatible epoxy (H2OE EPO-TEK), devices were affixed to clean pieces of aluminum foil and allowed to cure overnight at 65°C. In a glovebox attached to our cluster tool, epoxied samples were immersed in a bath of liquid nitrogen where they spontaneously cleaved. Each half was then withdrawn from the liquid nitrogen bath into a stream of dry nitrogen gas until it reached room temperature. Samples were loaded into the UHV transport system and the XPS system such that air exposure was avoided. Data were processed with PHI MultiPak v9.6 using standard elemental sensitivity factors. High-resolution XPS spectra were taken at a normal takeoff angle using monochromatic Al Kα radiation, with a pass energy of 1.75 eV, and in angle-integrating lens mode (±7°).

References

1. Luque, A. & Hegedus, S., editors. *Handbook of Photovoltaic Science and Engineering* (Wiley, Hoboken, NJ, 2011).
2. Gloeckler, M., Sankin, I., & Zhao, Z. CdTe solar cells at the threshold to 20% efficiency. *IEEE J. Photovolt*. **3**, 1389–1393 (2013).
3. Metzger, W.K., *et al.* Time-resolved photoluminescence studies of CdTe solar cells. *J. Appl. Phys.* **94**, 3549–3555 (2003).
4. Guo, J., Mannodi-Kanakkithodi, A., Sen F.G., Schwenker, E., Barnard, E.S., Munshi, A., Sampath, W., Shen, M.K.Y., & Klie, R. Effect of selenium and chlorine co-passivation in polycrystalline CdSeTe devices. *Applied Physics Letters* **115**, 153901 (2019).
5. Metzger, W.K., Grover, S., Lu, D., Colegrove, E., Moseley, J., Perkins, C.L., Li, X., Mallick, R., Zhang, W., Malik, R., *et al*. Exceeding 20% efficiency with in situ group V doping in polycrystalline CdTe solar cells. *Nat Energy* **4**, 837–845 (2019).
6. Metzger, W.K., Repins, I.L., & Contreras, M.A., Long Lifetimes in high-efficiency $Cu(In,Ga)Se_2$ solar cells. *Appl. Phys. Lett*. **93**, 022110 (2008).
7. deQuilettes, D.W., *et al.* Impact of microstructure on local carrier lifetime in perovskite solar cells. *Science* **348**, 683686 (2015).
8. Casey, H.C. & Stern, F. Concentration-dependent absorption and spontaneous emission of heavily doped GaAs. *J. Appl. Phys*. **47**, 631643 (1976).
9. Lush, G.B., Melloch, M.R., Lundstrom, M.S., Levi, D.H., Ahrenkiel, R.K., & MacMillan, H.F.

Microsecond lifetimes and low interface recombination velocities in moderately doped n-GaAs thin films. *Appl. Phys. Lett*. **61**, 2440–2442 (1992).
10. Niewelt, T., *et al*., Taking monocrystalline silicon to the ultimate lifetime limit, *Solar Energy Materials and Solar Cells* **185**, 252–259 (2018).
11. Best Research-Cell Efficiency Chart. https://www.nrel.gov/pv/cell-efficiency.html.
12. Duenow, J.N. & Metzger, W.K. Back-surface recombination, electron reflectors, and paths to 28% efficiency for thin-film photovoltaics: A CdTe case study. *J. Appl. Phys.* **125**, 053101 (2019).
13. Green, M.A., Dunlop, E.D., Hohl-Ebinger, J., Yoshita, M., Kopidakis, N., Ho-Baille, A.W.Y. Solar cell efficiency tables. *Prog. Photovolt. Res. Appl.* **28**, 3–15 (2020).
14. Wilson, G.M., *et al.* The 2020 Photovoltaics Technologies Roadmap. *J. Appl. Phys. D*, accepted (2020).
15. Lazard's Levelized Cost of Energy Analysis – Version 13.0; https://www.lazard.com/media/451086/lazards-levelized-cost-of-energy-version-130-vf.pdf
16. Britt, J. & Ferekides, C. Thin-film CdS/CdTe solar cell with 15.8% efficiency. *Appl. Phys. Lett.* **62**, 2851 (1993).
17. Wu, X. High-efficiency polycrystalline CdTe thin-film solar cells. *Solar Energy* **77**, 803–814 (2004).
18. Wu, X., *et al.* Phase control of Cu_xTe film and its effects on CdS/CdTe solar cell, *Thin Solid Films* **515**, 5798–5803 (2007).
19. Duggal, A.R., Shiang, J.J., Huber, & W.H., Halverson, A.F. US 2014/0373908 (2014).
20. Munshi, A.H., Kephart, J., Abbas, A., Raguse, J., Beaudry, J.N., Barth, K., Sites, J., Walls, J. & Sampath, W. Polycrystalline CdSeTe/CdTe absorber cells with 28 mA/cm^2 short-circuit current. *IEEE Journal of Photovoltaics* **8**, 310–314 (2018).
21. Zheng, X., *et al.* Recombination and bandgap engineering in CdSeTe/CdTe solar cells. *Appl. Phys. Lett. Materials* **7**, 071112 (2019).
22. Fiducia, T.A.M., Mendis, B.G., Li, K., Grovenor, C.R.M., Munshi A.H., Barth, K., Sampath, W.S., Wright, L.D. Abbas A., & Walls, J.M. Understanding the role of selenium in defect passivation for highly efficient selenium-alloyed cadmium telluride solar cells. *Nature Energy* **4**, 504–511, 2019.
23. Zheng. X., *et al*., under review.
24. Major, J.D., Treharne, R.E., Phillips, L.J., & Durose, K. A low-cost non-toxic post-growth activation step for CdTe solar cells. *Nature* **511**, 334–337 (2014).
25. Poplawsky, J.D., Guo, W., Paudel, N., Ng, A., More, K., Leonard, D., & Yan, Y. Structural and compositional dependence of the $CdTe_xSe_{1-x}$ alloy layer photoactivity in CdTe-based solar cells. *Nature Communications* **7**, 1–9 (2016).
26. Moseley, J., *et al.* Recombination by grain-boundary type in CdTe, *J. Appl. Phys.* **118**, 025702 (2015).
27. Burst, J.M., *et al.* CdTe solar cells with open-circuit voltage breaking the 1 V barrier. *Nat. Energy* **1**, 16015 (2016).
28. Jensen, S.A., *et al*. Long carrier lifetimes in large-grain polycrystalline CdTe without $CdCl_2$. *Appl. Phys. Lett*. **108**, 263903 (2016).
29. Kephart, J.M., Kindvall, A., Williams, D., Kuciauskas, D., Dippo, P., Munshi, A., & Sampath, W.S. Sputter-deposited oxides for interface passivation of CdTe photovoltaics. *IEEE J. Photovolt.* **8**, 587–593 (2018).
30. Ablekim, T., *et al.* Tailoring MgZnO/CdSeTe interfaces for photovoltaics. *IEEE J. Photovolt.* **9**, 888–892 (2019).
31. O'Connor, D.V. & Phillips, D. Time-Correlated Single Photon Counting (Academic Press, 1984).
32. Metzger, W.K., Ahrenkiel, R.K., Dashdorj, J., & Friedman, D.J. Analysis of charge separation dynamics in a semiconductor junction. *Phys. Rev. B* **71**, 03530 (2005).
33. Metzger, W.K., Romero, M.J., Dippo, P., & Young, M. Characterizing recombination in CdTe solar cells with time-resolved photoluminescence. In *Proc. 2006 IEEE 4th World Conference on Photovoltaic Energy Conference* 372–375 (IEEE, 2006).
34. Ahrenkiel, R.K. & Lundstrom, M.S. Minority Carriers in III-V Semiconductors: Physics and Applications (Academic Press, 1993).
35. Fahrenbruch, A.L., & Bube, R.H. Fundamentals of Solar Cells: Photovoltaic Solar Energy Conversion

(Academic Press, 1983).
36. McGott, D.L., Thermomechanical lift-off and recontacting of CdTe solar cells, *ACS Appl. Mater. Interfaces* **10**, 44854–44861 (2018).
37. Perkins, C.L., McGott, D.L., Reese, M.O., & Metzger, W.K. SnO_2-catalyzed oxidation in high-efficiency CdTe solar cells. *ACS Appl. Mater. Interfaces* **11**, 13003–13010 (2019).
38. Carmona-Rodriguez, J., Lozada-Morales, R., Jiménez-Sandoval, O., Rodríguez-Melgarejo, F., Meléndez-Lira, M., & Jiménez-Sandoval, S.J. $CdTeO_x$ to $CdTeO_3$ structural phase transition in as-grown polycrystalline films by reactive sputtering. *J. Appl. Phys*. **103**, 123516 (2008).
39. Moseley, J., Guthrey, H., Al-Jassim, M., & Metzger, W.K. in *Physics, Simulation, and Photonic Engineering of Photovoltaic Devices VIII.* 109130Z (International Society for Optics and Photonics).
40. Metzger, W.K. & Gloeckler, M. The impact of charged grain boundaries on thin-film solar cells and characterization. *J. Appl. Phys*. **98**, 063701 (2005).
41. Munroe, P.R. The application of focused ion beam microscopy in the material sciences. *Mater. Charact.* **60**, 2–13 (2009).
42. Abou-Ras, D., Kirchartz, T., & Rau, U. Advanced Characterization Techniques for Thin Film Solar Cells (John Wiley & Sons, 2016).
43. Moseley, J.M., *et al.*, Luminescence methodology to determine grain-boundary, grain-interior, and surface recombination in thin-film solar cells, *J. Appl. Phys*. **124**, 113104 (2018).
43. Perkins, C.L. Molecular anchors for self-assembled monolayers on ZnO: A direct comparison of the thiol and phosphonic acid moieties. *J. Phys. Chem. C* **113**, 18276–18286 (2009).

Acknowledgments: This work was authored in part by the National Renewable Energy Laboratory, operated by Alliance for Sustainable Energy, LLC, for the U.S. Department of Energy (DOE) under Contract No. DE-AC36-08GO28308. Funding provided by the U.S. Department of Energy Office of Energy Efficiency and Renewable Energy Solar Energy Technologies Office and CRD-13-507. The views expressed in the article do not necessarily represent the views of the DOE or the U.S. Government.

Competing Interests: T.A. currently works at First Solar, which is a publicly traded company that manufactures CdTe solar panels and develops grid-connected photovoltaic power plants. Outside of this and the funding listed in the acknowledgments section, the authors declare no competing interests.

.

Data Availability: The data that support the plots within this article are available from the authors upon reasonable request.

Author Contributions: T.A., J.D., X.Z., M.O.R., M.A., and E.C. performed film and device synthesis as well as JV and QE measurements. C.L.P., J.M., S.C., T.B., B.F., and S.J. performed XPS, CL, and TRPL measurements. T.A. and W.K.M. directed research. All authors contributed to the design and interpretation of experiments and the manuscript.

Corresponding author: W.K.M. is the corresponding author and can be contacted at Wyatt.Metzger@nrel.gov